Taxol-stabilized microtubules promote the formation of filaments from unmodified full-length Tau in vitro

Aranda R. Duan and Holly V. Goodson
Department of Chemistry and Biochemistry, University of Notre Dame, Notre Dame, IN 46556

ABSTRACT **Tau is a neuronal protein that stabilizes the microtubule (MT) network, but it also forms filaments associated with Alzheimer's disease. Understanding Tau–MT and Tau–Tau interactions would help to establish Tau function in health and disease. For many years, literature reports on Tau–MT binding behavior and affinity have remained surprisingly contradictory (e.g., 10-fold variation in Tau–MT affinity). Tau–Tau interactions have also been investigated, but whether MTs might affect Tau filament formation is unknown. We have addressed these issues through binding assays and microscopy. We assessed Tau–MT interactions via cosedimentation and found that the measured affinity of Tau varies greatly, depending on the experimental design and the protein concentrations used. To investigate this dependence, we used fluorescence microscopy to examine Tau–MT binding. Strikingly, we found that Taxol-stabilized MTs promote Tau filament formation without characterized Tau-filament inducers. We propose that these novel Tau filaments account for the incongruence in Tau–MT affinity measurements. Moreover, electron microscopy reveals that these filaments appear similar to the heparin-induced Alzheimer's model. These observations suggest that the MT-induced Tau filaments provide a new model for Alzheimer's studies and that MTs might play a role in the formation of Alzheimer's-associated neurofibrillary tangles.**

Monitoring Editor
Monica Bettencourt-Dias
Instituto Gulbenkian de Ciência

Received: May 15, 2012
Revised: Oct 9, 2012
Accepted: Oct 11, 2012

INTRODUCTION

Tau protein is expressed in neurons and functions to stabilize microtubules (MTs; Makrides *et al.*, 2004; Choi *et al.*, 2009). MTs are dynamic polymers, able to grow and shrink, and these dynamics are regulated by a group of MT-associated proteins, including Tau (Desai and Mitchison, 1997; Amos, 2000; Askham and Morrison, 2002; Howard and Hyman, 2003). In neurons, MTs are linearly and densely packed along the length of the axon, inducing a global cellular polarity critical for neuronal signaling (Tanaka and Kirschner, 1991; Slaughter *et al.*, 1997; Witte *et al.*, 2008). In normal cells, Tau is found distributed throughout axons and is localized to MTs. The interaction of Tau with MTs is regulated through many mechanisms, including alternative splicing (there are six known human Tau isoforms) and phosphorylation (Alonso *et al.*, 2010; Fauquant *et al.*, 2011). However, in Alzheimer's disease, Tau becomes aggregated to form neurofibrillary tangles (NFTs), and it is no longer associated with the MT network (Goedert *et al.*, 1999; Sun and Gamblin, 2009). The Tau in these tangles is quite different from that in normal cells, in that it is hyperphosphorylated and has a different ratio of expressed isoforms. It is also structurally altered: normal Tau is soluble with very little secondary structure, but Tau molecules in NFTs bind together to form straight, ribbon-like filaments or paired helical filaments with beta-sheet content (Mizushima *et al.*, 2007; Jeganathan *et al.*, 2008).

As yet, it is not clear whether the formation of NFTs is a cause or effect of Alzheimer's, but the correlation between Tau-rich NFTs and Alzheimer's has made Tau a target of much research. One focus has been on studying interactions between MTs and Tau, with the goal of establishing the normal physiological function of the protein. This work has shown that Tau promotes MT

This article was published online ahead of print in MBoC in Press (http://www.molbiolcell.org/cgi/doi/10.1091/mbc.E12-05-0374) on October 19, 2012.

Address correspondence to: Holly V. Goodson (hgoodson@nd.edu).

Abbreviations used: EM, electron microscopy; MT, microtubule; NA, numerical aperture; NFT, neurofibrillary tangle; TcMv, Tau constant MT varied; TEM, transmission electron microscopy; TvMc, Tau varied MT constant.

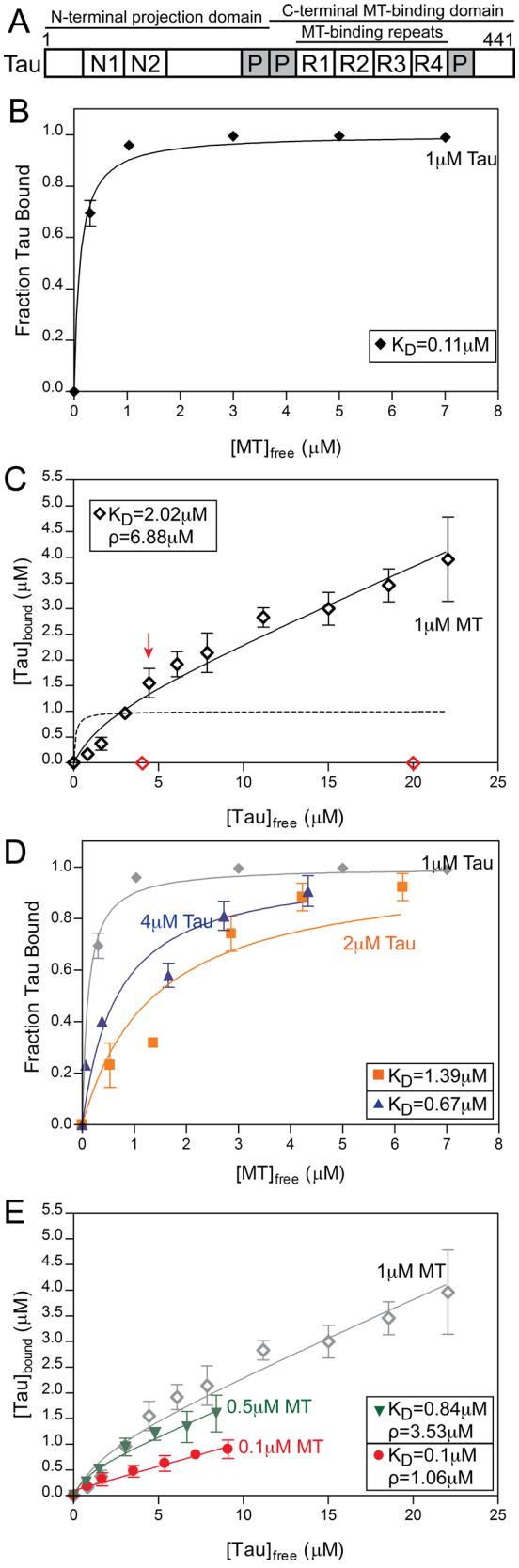

FIGURE 1: The apparent Tau–MT affinity depends on the methods and protein concentrations used. (A) Schematic diagram of the domains of the full-length Tau used in this study (441 amino acids, not drawn to scale). The C-terminus contains four MT-binding repeat motifs (R1–R4) surrounded by proline-rich regions (P). (B) Tau–MT binding behavior determined according to approach TcMv, with total MT concentrations ranging from 0 to 8 μM (see *Materials and Methods*). When the data were fitted (solid line) using nonlinear regression according to the standard binding equation (Eq. 1; see Appendix), a K_D of 0.11 ± 0.02 μM was obtained. (C) Tau–MT binding behavior determined according to approach TvMc, with total Tau concentrations ranging from 0 to 26 μM. The dotted line shows a theoretical curve plotted according to Eq. 2 using the K_D value calculated in (B); the data are clearly inconsistent with this curve. The solid line shows a fit of the data to Eq. 3, which includes an additional linear term meant to account for Tau–Tau interactions on the MTs (see the Appendix). According to this fit, K_D = 2.02 ± 1.03 μM and ρ = 6.88 ± 0.37 μM. The red arrow indicates the point at which supersaturation (greater than 1:1 binding) begins to occur, and the red data points show the sedimentation behavior of moderate (4 μM) and high (20 μM) concentrations of Tau in the absence of MTs. (D) Approach TcMv at 2 μM (orange) and 4 μM (blue) Tau, with total MT concentrations ranging from 0 to 8 μM. When these data were fitted to the standard binding equation (Eq. 1), K_D values of 1.39 ± 0.35 μM and 0.67 ± 0.16 μM for 2 and 4 μM Tau, respectively, were obtained. The gray data and curve are reproduced from (B) and are provided for comparison. The variability in the data at higher [Tau] is discussed in the Appendix. (E) Approach TvMc at 0.5 μM (green) and 0.1 μM (red) MT, with total Tau concentrations ranging from 0 to 10 μM. When these data were fitted to Eq. 3 (see Appendix), the following values were obtained: for 0.5 μM MT, K_D = 0.84 ± 0.41 μM and ρ = 3.53 ± 0.21 μM, while for 0.1 μM MT, K_D = 0.10 ± 0.32 μM and ρ = 1.06 ± 0.04 μM. The gray data and curve are reproduced from (C) and are provided for comparison. Data in all panels are the average of ≥3 trials ± SD.

stability and reduces MT dynamics (Panda *et al.*, 1995; Al-Bassam *et al.*, 2002; Bunker *et al.*, 2004). The MT-binding and MT-stabilizing activities of Tau are contained within the C-terminal domain, which contains four MT-binding repeat motifs sandwiched by proline-rich regions (Figure 1A). The N-terminus of Tau (also called the projection domain) is believed to space apart MTs within the crowded axon by bridging with the Tau N-termini projecting from neighboring MTs (Hirokawa *et al.*, 1988; Kempf *et al.*, 1996). While there is general agreement about these aspects of Tau–MT interactions, the literature contains conflicting information about others. As previously noted by Ackmann and colleagues, the reported values for the Tau–MT affinity vary by more than an order of magnitude, from less than 100 nM to more than 1 μM (Goode and Feinstein, 1994; Ackmann *et al.*, 2000; Makrides *et al.*, 2004). Research has shown that different isoforms have different affinities, but wide ranges of affinities have been reported, even for the same isoform (Goode and Feinstein, 1994; Sillen *et al.*, 2007; Fauquant *et al.*, 2011), and the origin of these discrepancies remains unresolved.

Another research focus has been on understanding the process of NFT formation. Because the Tau in Alzheimer's NFTs is highly phosphorylated and does not bind to MTs (Paudel and Li, 1999; Alonso *et al.*, 2010), in vitro studies of NFT formation have generally utilized systems devoid of MTs. These studies have concluded that unmodified Tau can form filaments similar to Alzheimer's NFTs in vitro, but that the process requires a lot of time (days) and the presence of promoters, such as heparin, arachidonic acid, or polyglutamates (Friedhoff *et al.*, 1998; Barghorn and Mandelkow, 2002; Hiraoka *et al.*, 2004; Jeganathan *et al.*, 2008). Some previous studies have shown that Tau–Tau oligomerization can occur in the presence of MTs and even that Tau–Tau oligomerization is promoted

by MTs (Ackmann *et al.*, 2000; Makrides *et al.*, 2003). On the basis of these observations, researchers have concluded that Tau can bind to the subset of Tau molecules that are bound to MTs (Ackmann *et al.*, 2000; Makrides *et al.*, 2003; Sillen *et al.*, 2007). However, while there is clear evidence that MTs promote Tau oligomerization on the surface of MTs, to our knowledge, no studies have investigated whether Tau filament formation might be influenced by the presence of MTs.

In the course of other experiments, we became puzzled by the surprising range of reported Tau–MT affinity values. We decided to investigate the possibility that differences in experimental approach could explain (at least partially) the discrepancies in the values of the reported dissociation constant. MT-binding studies are typically performed using cosedimentation assays in which the [Tau] is held constant and the [polymerized tubulin] is varied, or alternatively where [polymerized tubulin] is held constant and [Tau] is varied. In either case, the amount of Tau that cosediments with the MTs is interpreted as Tau that is bound to MTs. By performing experiments in which we used both experimental designs in parallel, we found that the apparent affinity of Tau for MTs depends both on the approach used to study the interaction and on the concentration of each binding partner. We found that this dependence is observed when the data are fitted using both standard binding models or binding models designed to account for Tau–Tau oligomerization at the MT surface, suggesting that an interaction not accounted for by these models is occurring in these reactions.

To investigate this question, we used fluorescence microscopy to examine the behavior of labeled Tau in the presence and absence of MTs. Surprisingly, we found that MTs induce the rapid formation of Tau-only filaments. This observation is important for two reasons. First, the existence of these filaments confounds attempts to measure Tau–MT interactions by any method, because they deplete the pool of free Tau available to bind to MTs, and they spin down in cosedimentation assays. More significantly, these filaments form in regular MT-binding buffers, are induced by MTs, and are seen by electron microscopy (EM) to be similar to the well-established Alzheimer's-like Tau filaments induced by heparin. These observations suggest that the MT-induced filaments might provide a useful new in vitro model for the formation of Tau filaments in Alzheimer's disease, and they raise the possibility that MTs play a previously unappreciated role in the formation of Alzheimer's-associated NFTs.

Our article is divided into two sections. The first focuses on measuring the Tau–MT binding affinity, as estimated by different experimental approaches and binding models, and on the failure of any of the commonly used binding models to fit the range of data. An overview of the experiments and interpretations is provided in the main text, while a more detailed discussion can be found in the Appendix. The second section focuses on the observation that MTs induce the formation of Tau filaments.

RESULTS AND DISCUSSION

Investigations of Tau–MT interactions

To elucidate the origin of the inconsistencies in the reported Tau–MT affinity values (Goode and Feinstein, 1994; Ackmann *et al.*, 2000; Makrides *et al.*, 2004), we first investigated the possibility that different experimental designs yield different apparent dissociation constants. In measuring dissociation constants, the researcher usually holds one protein constant, while varying the concentration of the other, and then evaluates the amount of complex formed under each condition. As noted above, binding to MTs is typically assessed by cosedimentation, in which the experimenter assumes that the reaction has reached equilibrium and that any test protein that sediments does so by binding to the MTs. In some analyses of Tau–MT binding, researchers hold Tau constant, while varying the concentration of polymerized tubulin (e.g., Goode and Feinstein, 1994). In others, polymerized tubulin is held constant, while Tau is varied (e.g., Ackmann *et al.*, 2000). We refer to these approaches as "Tau constant MT varied" (TcMv) and "Tau varied MT constant" (TvMc), respectively (see *Materials and Methods*). To test whether differences between TcMv and TvMc could account for the differences in published Tau–MT affinity values, we measured Tau–MT interactions using both approaches under otherwise identical conditions.

As shown in Figure 1 and discussed more in the Appendix, the apparent affinity of Tau for Taxol-stabilized MTs depends on the method used to assess the interaction (Figure 1, compare B and C). The measured affinity also depends on the concentration of Tau used in the assay (Figure 1D). This dependence on [Tau] is expected, based on previous experiments that were interpreted as showing that Tau binds to MT-bound Tau (Ackmann *et al.*, 2000; Makrides *et al.*, 2003). It also provides an explanation for the observation that the apparent affinity depends on the approach used to assess the interaction, because [Tau] is held constant in approach TcMv and varies in approach TvMc.

Ackmann and colleagues generated a binding model that attempts to account for both Tau–MT interactions and the binding of Tau to MT-bound Tau (Ackmann *et al.*, 2000). In this model, the Tau–MT dissociation constant could be calculated from the fit of their equation to the binding data. However, contrary to the predictions of this model, we observed that the apparent affinity of Tau for MTs also depends on the concentration of MTs (Figure 1E). This observation suggests that an as yet unaccounted for reaction is occurring in the Tau–MT binding assays, and it led us to consider the possibility that Tau might be forming filaments in our MT-binding assays (for a more in-depth discussion of these experiments and their interpretations, see Appendix).

Investigations of Tau–Tau interactions: MTs induce the formation of Tau filaments

It is well-established that Tau forms filaments under pathological conditions (e.g., Alzheimer's disease) and that solutions of purified Tau form filaments in vitro upon exposure of a Tau solution to inducers, such as heparin (Jeganathan *et al.*, 2008; Wegmann *et al.*, 2011). As discussed above, it is also accepted that Tau can engage in Tau–Tau interactions on the MT surface (Ackmann *et al.*, 2000; Kar *et al.*, 2003; Makrides *et al.*, 2003). We wondered whether the unusual behavior of Tau in the MT-binding assays might be caused at least in part by the formation of Tau filaments during the assays. Such an observation would be surprising, because formation of heparin-induced Tau filaments is very slow, taking days to accumulate significant concentrations of filaments, and is normally performed at much higher [Tau] than used in our experiments. However, we decided that it was worthwhile to investigate, because, as discussed above, the dependence of the apparent Tau–MT K_D on the concentration of MTs was inconsistent with Ackmann's mathematical model for Tau–MT interactions. Moreover, the Tau in our TvMc assays appeared to be cosedimenting with MTs at levels beyond what could be explained solely by limited Tau oligomerization at the MT surface, as predicted using the mathematical models of MTBindingSim (Philip *et al.*, 2012; unpublished data). These observations suggested that we should investigate the possibility that MTs induce the formation of Tau filaments.

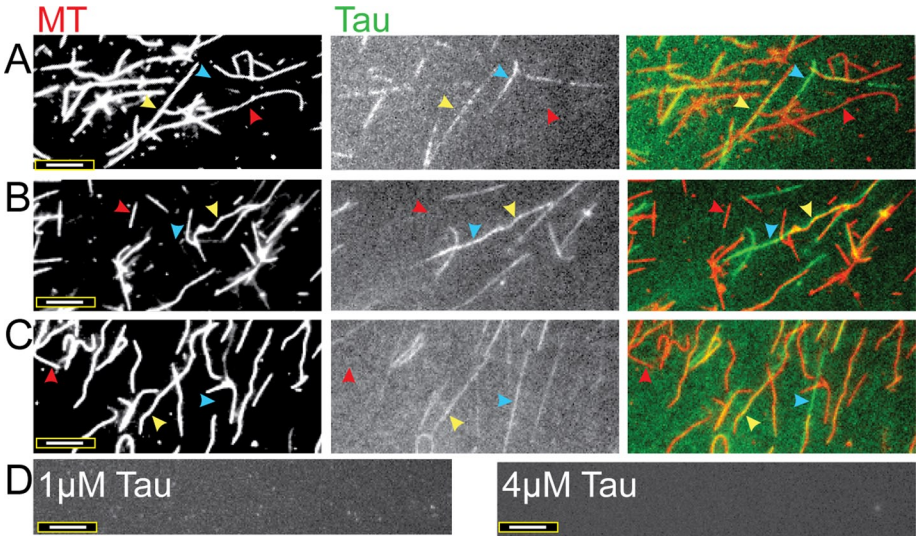

FIGURE 2: Fluorescently labeled Tau and MTs reveal sporadic Tau–MT decoration and the formation of Tau filaments. Incubations of (A) 1 μM Tau:4 μM MTs, (B) 2 μM Tau:4 μM MTs, and (C) 4 μM Tau:4 μM MTs for 15 min at 37°C. Individual MTs vary from being sparsely decorated with Tau (red arrowheads) to being moderately and heavily decorated with Tau (yellow arrowheads). Tau filaments that are not associated with MTs are also evident (blue arrowheads). In the right-most panels, colored images display tubulin as red and Tau as green; the overlay of Tau and tubulin appears as yellow. (D) The results of control experiments performed with Tau protein alone at low (1 μM) and high (4 μM) concentrations, in which no Tau filaments are observed. Scale bars: 8 μm. The images shown represent the typical results of more than 10 independent experiments performed with Tau from multiple purifications and labeling reactions.

Cross-linking supports the existence of Tau–Tau interactions in the MT-binding assays

Our first goal in testing the hypothesis that filaments might be forming in our assays was to reproduce the results of Makrides *et al.* (2003), who showed that MTs promote the formation of cross-linkable Tau–Tau complexes that were interpreted as evidence that MTs promote the formation of Tau oligomers. Supplemental Figure S1 provides evidence that Tau does cross-link to Tau in our assays and, as expected, does so only in the presence of MTs (Figure S1). While encouraging, these experiments did not reveal whether the Tau–Tau interactions are occurring in a limited way on the MT surface, consistent with previous understanding, or might be occurring as part of a previously unrecognized polymerization process.

Novel Tau filament formation revealed by fluorescence microscopy

To more directly investigate the possibility that the Tau in our assays was forming filaments, we turned to fluorescence microscopy. More specifically, we performed experiments in which we added varying amounts of Alexa Fluor–labeled Tau (1–4 μM) to a constant amount of rhodamine-labeled MTs (4 μM), incubated the mixtures for 15 min (similar to the cosedimentation assays), and imaged the samples at the appropriate wavelengths. The first thing we noticed was that the Tau decorated the MTs very unevenly: some MTs were well-decorated, some appeared to be lacking Tau entirely, and others were sporadically decorated (Figure 2). Atomic force microscopy work performed by Schaap *et al.* (2007) also showed sporadic Tau decoration on MTs.

However, the more striking observation is the appearance of filaments that appear to be composed of Tau alone: in the right panels of Figure 2, one can see green Tau-labeled filaments (blue arrowheads) that do not correspond at all to the position of MTs in the left panels (Figure 2). Importantly, the assembly of these Tau-only filaments requires the presence of MTs: we saw no such Tau-only filaments form under otherwise identical conditions in the absence of MTs (Figure 2D). The number of these Tau-only filaments also seems to depend on the different Tau concentrations used (Figure 2). Furthermore, we found that the Tau-only filaments remained intact after we allowed the MTs to depolymerize by lengthy incubations in buffer without Taxol (Figure 3). This observation indicates that while the Tau filaments do require MTs to form (Figure 2), they do not require MTs to be maintained.

Effect of Tau filament formation on measuring Tau–MT affinity

The formation of MT-induced Tau filaments could interfere with MT-binding assays in two different ways that would be reflected in the binding data found in Figure 1. First, the Tau filaments could cosediment with MTs, either by being associated with MTs or by sedimenting independently. If the Tau filaments cosediment, filament formation is expected to increase both the apparent affinity and the apparent Tau_{bound}:tubulin ratio by increasing the fraction of Tau that sediments at a given concentration. To test the hypothesis that the Tau filaments do cosediment with MTs, we incubated fluorescently labeled 2 μM Tau and 4 μM MTs for 15 min at 37°C and performed a standard cosedimentation assay. However, this time, instead of loading the supernatant and pellet fractions on a gel, we imaged them using fluorescence microscopy. We observed that both MTs and Tau filaments sediment nearly to completion—few of either were found in the supernatant (Figure 4). These data show that the central assumption of cosedimentation assays (the idea that Tau in the pellet is bound to MTs) is being violated under any condition in which the Tau filaments are being formed. Thus cosedimentation assays cannot be used to provide a valid measurement of Tau–MT interactions if filaments are present.

Because Tau filament sedimentation perturbs affinity measurements, our initial conclusion was that this problem likely accounts for the failure of binding models to match the data, and that we needed to find a different technique (one that did not use sedimentation) to measure Tau–MT interactions. However, we realized that no approach would be sufficient to provide a valid measurement, because the formation of Tau filaments perturbs affinity measurements in a second way as well: assembly of Tau into filaments depletes the pool of free Tau available to bind to MTs, which would decrease the apparent affinity by decreasing the effective concentration of Tau present in a given reaction. While the first problem (sedimentation of Tau filaments) is specific to cosedimentation assays, the second problem (depletion of the pool of free Tau) impacts any technique that can be used to measure Tau–MT interactions, regardless of whether sedimentation is involved.

Therefore we decided to see whether there was a Tau concentration at which filament formation was minimal over the relevant range of MT concentrations. Our expectation was that identifying such a concentration would allow for a nonperturbed measurement of Tau–MT interactions. Experiments in which we varied the concentration of Tau incubated with 4 μM MTs showed that 1 μM Tau formed relatively few filaments (Figure 5). This observation indicates that the

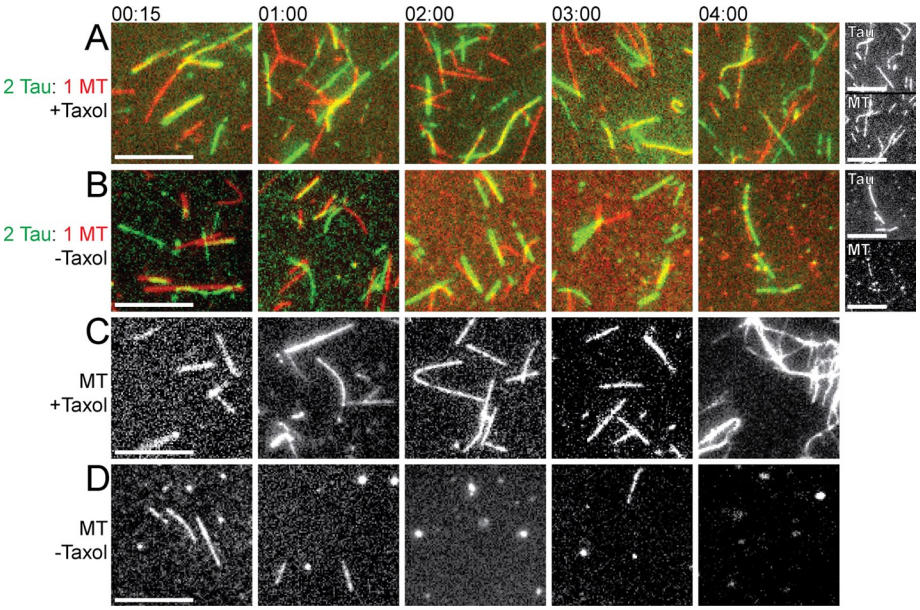

FIGURE 3: Tau filaments form in the presence of MTs and remain after MTs dissociate. MTs (4 μM) were incubated at 37°C in the absence or presence of Tau (2 μM) and/or the MT-stabilizing drug Taxol (10 μM). Samples of the incubations were taken at different time intervals (from 15 min to 4 h, as indicated) and imaged. Colored images display tubulin as red and Tau as green and their overlay as yellow. Scale bars: 8 μm. (A) MTs incubated with Taxol and Tau; the far right pair of panels shows grayscale images for the 4-h time point. (B) MTs incubated with Tau in the absence of Taxol; the far right pair of panels shows grayscale images for the 4-h time point. (C) MTs incubated alone with Taxol. (D) MTs incubated without Taxol or Tau. Note that MTs without Taxol dissociate over time (more slowly when Tau is present), but the Tau filaments remain. Images shown represent the typical results of more than six different fields of collected data.

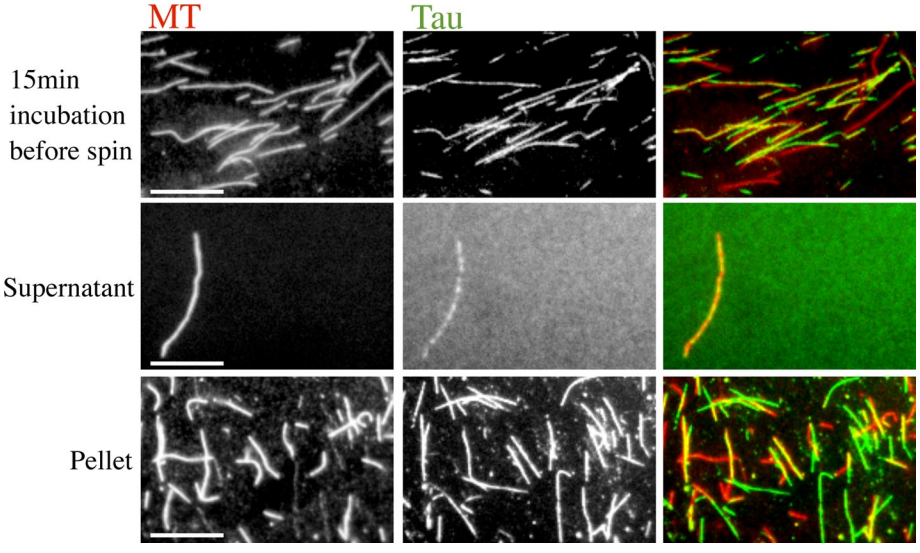

FIGURE 4: Tau filaments spin down in ultracentrifugation. Tau (2 μM) and MTs (4 μM) were incubated at 37°C for 15 min. The mixture was ultracentrifuged, and the supernatant and pellet were separated according to MT-binding assay protocol for imaging. While the "before spin" and pellet images are representative, the supernatant image shows one of very few MTs left in the supernatant. These data show that cosedimentation assays are likely to yield invalid measurements of the Tau–MT affinity, because cosedimentation assumes that all Tau in the pellet is bound to MTs. Colored images display tubulin as red and Tau as green and their overlay as yellow. Scale bars: 10 μm. Images shown represent the typical results of three independent experiments.

dissociation constant measured in Figure 1B likely provides a reasonable estimate of the actual Tau–MT dissociation constant in agreement with previous measurements performed at low [Tau], e.g., Goode and Feinstein (1994). Moreover, it suggests that other measurements of Tau–MT affinity should be performed at a similarly low Tau concentration, unless conditions are found under which filament formation does not occur.

Two remaining issues are the surprising variability in the fraction of Tau that sediments in Figure 1D and the inconsistent trend in apparent affinity when Tau increases from 1 to 2 and 4 μM. We hypothesized that one reason for the variability might be that Tau polymerization takes longer than 15 min to reach its endpoint and that small differences in the nucleation process or the incubation time would vary the amount of polymerized Tau within this short time frame. To test this hypothesis, we incubated the Tau with MTs for a longer time and collected images at different time points. Working with 2 μM Tau and 4 μM MTs, we found that Tau starts out in both MT-bound and Tau filament form at 15 min, but shifts completely into Tau filament form after 1 h (Figure 6). After 60 min, the Tau is found mostly in Tau filament form and the MTs are largely undecorated; only relatively few MTs have Tau bound in a very heavily decorated manner (Figure 6).

To assess the impact of this time-dependent polymerization on the cosedimentation assays, we repeated the 2 μM Tau TcMv experiments of Figure 1D by incubating the Tau–MT mixture for 1 h instead of 15 min. Consistent with the observations of Figures 4 and 6, we saw that all of the Tau shifted to the pellet as long as MTs were present (see Figure S2), making it appear that the increased incubation time shifted the Tau–MT interaction from a low binding affinity to a high binding affinity. However, this would be an incorrect interpretation: Tau sedimentation results from a combination of fast MT binding and slower Tau polymerization. One impact of this sedimentation behavior is that the apparent affinities obtained from the experiments of Figure 1D are not legitimate measurements of the Tau–MT binding interaction. Moreover, because the kinetics of the Tau polymerization process likely vary in a complicated way with the number of nucleation sites, this time-dependent polymerization behavior also provides an explanation for the variability seen at particular MT concentrations. These issues require further study.

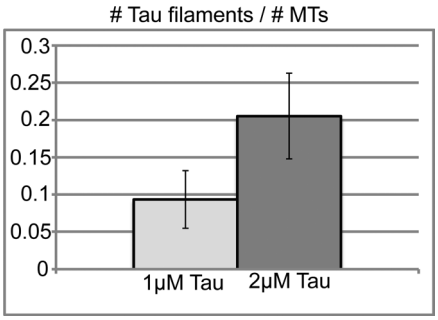

FIGURE 5: Experiments using 1 μM Tau minimize Tau filament formation. Tau (1 or 2 μM) was incubated for 15 min at 37°C with 4 μM MTs, and then the solution was imaged by fluorescence microscopy. The number of MTs and Tau filaments were counted from three separate optical fields spanning a total imaged area of 35.6 square mm under each condition. The number of MTs counted exceeded 300 within each field. The fields chosen for counting were typical representations of more than 10 experiments.

Investigations into how MTs nucleate Tau filaments

The observation that Tau filaments do not form in the absence of MTs or other inducers indicates that Tau polymerization (also called fibrillization) is a nucleation-limited process. One obvious question

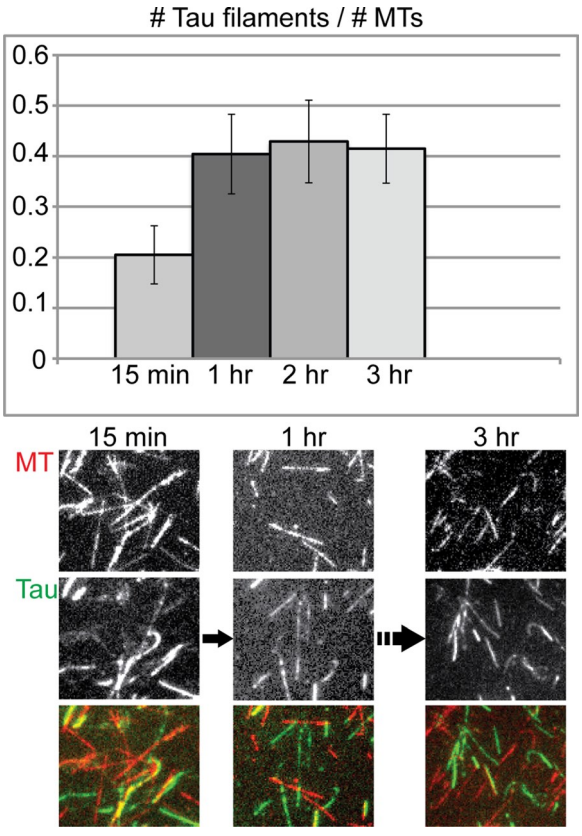

FIGURE 6: Formation of Tau filaments is a time-dependent process. Tau (2 μM) was incubated with 4 μM MTs periodically supplemented with Taxol at 37°C, and images were collected at 15-min, 1-h, 2-h, and 3-h time points. By 1 h, the number of Tau filaments had reached a maximum. The bar graph data were generated as described in Figure 5, counted from three separate optical fields spanning a total imaged area of 35.6 square mm. The number of MTs counted exceeded 300 within each field. The fields chosen for counting are typical representations of more than six different fields of collected data.

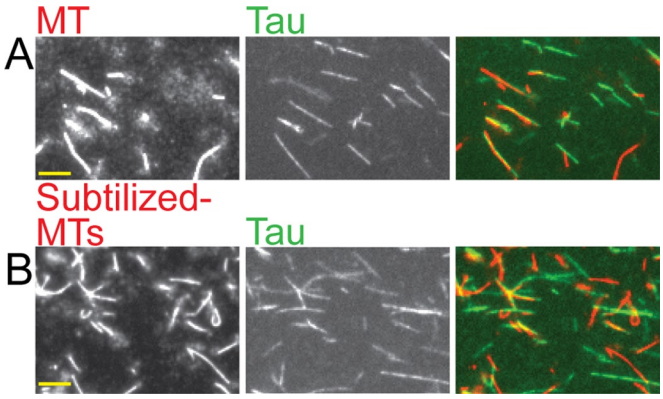

FIGURE 7: Subtilisin-treated MTs can promote the formation of Tau filaments. (A) Tau (2 μM) incubated with 4 μM normal Taxol-stabilized MTs for 15 min. (B) Tau (2 μM) incubated for 15 min with 4 μM subtilized MTs that have both C-terminal tubulin tails cleaved (tested by Western blot analysis; see Figure S3). Left panels show MTs, middle panels show Tau, and the right panels show the overlay; the MTs are displayed in red, the Tau in green, and the overlay in yellow. Scale bar: 10 μm. Images shown represent the typical results of more than 30 different fields of collected data.

is how MTs promote the formation of Tau filament nuclei. We first hypothesized that this process might be promoted by the glutamate-rich C-terminal tails of tubulin, since polyglutamates can induce Tau fibrillization in vitro (Friedhoff *et al.*, 1998). To test this idea, we incubated Tau with MTs from which the α- and β-tails of the tubulin dimers had been removed by subtilisin digestion (Figures 7 and S3). Surprisingly, we found that when we used MTs stripped of their glutamate-rich tails, there was no obvious effect on formation of the Tau filaments (Figure 7).

This observation indicates that the tubulin tails are not involved in the nucleation process, but does not provide any information about what aspect of the MT structure is involved. Further work will be required to resolve this question. However, one speculation is that the filaments might be nucleated by MT tips, as suggested by fluorescence microscopy images showing Tau filaments extending from MT tips (Figure S4). We used EM to better visualize the Tau filaments and perhaps gain insight into the nucleation mechanism, as discussed in the following section.

Possible relationship of MT-induced Tau filaments to Tau NFTs

Up to now, the only in vitro experimental model for the formation of Tau NFTs seen in Alzheimer's disease has been the assembly of Tau filaments by inducers, such as heparin, arachidonic acid, and polyglutamates (e.g., Friedhoff *et al.*, 1998; Jeganathan *et al.*, 2008). Heparin fibrillizes full-length human Tau into a combination of twisted and flat, ribbon-like filaments. EM, thioflavin-S fluorescence, Fourier transform infrared spectroscopy, and circular dichroism studies have provided evidence that these filaments can be used as an acceptable model of the NFTs that form in Alzheimer's disease (Ramachandran and Udgaonkar, 2011; Wegmann *et al.*, 2011). As noted earlier, this filament assembly typically occurs over a period of days or at least hours, often uses very high Tau concentrations, requires anionic inducers, and is performed in systems devoid of MTs. To investigate the relationship between our novel Tau filaments and the heparin-induced filaments used as models for NFTs, we turned to transmission electron microscopy (TEM).

We prepared samples made with MTs alone, Tau alone, and mixtures of MTs and Tau under the same conditions as used for the

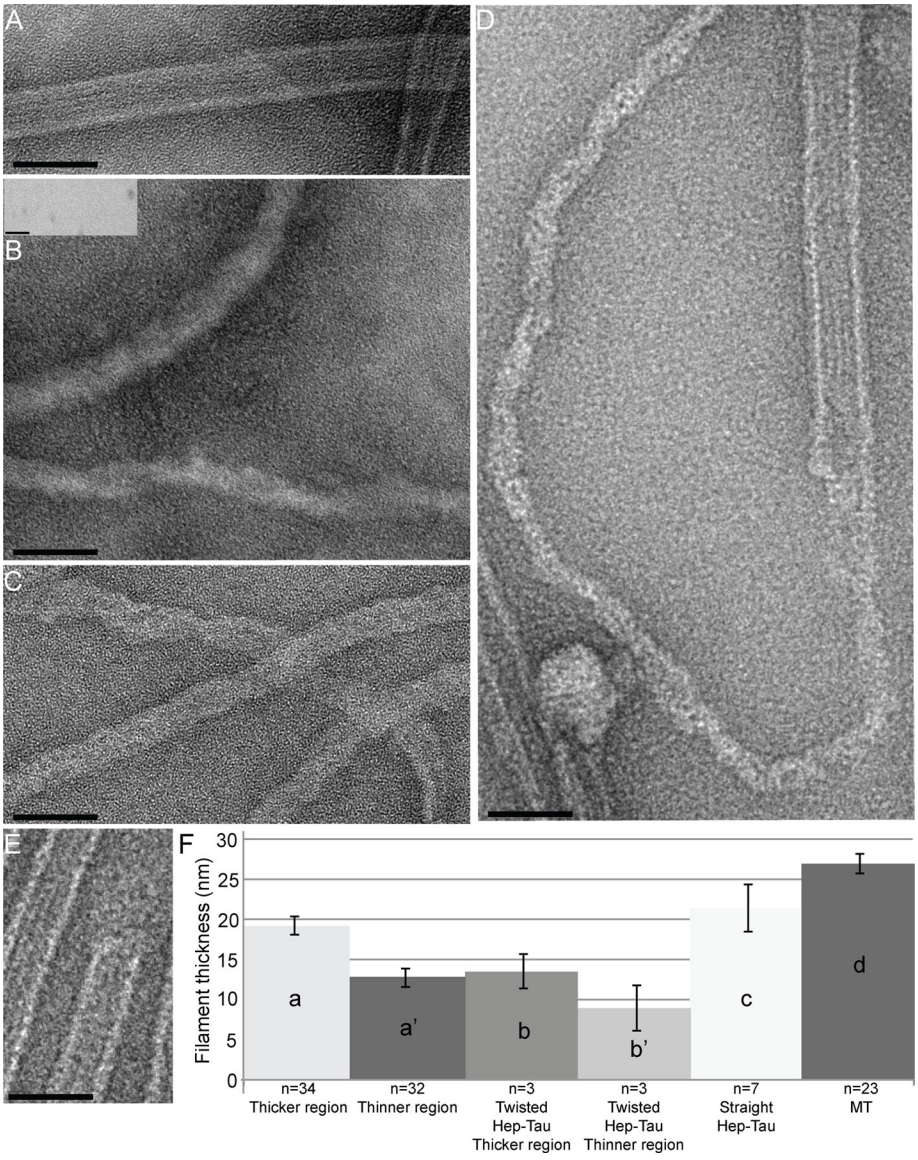

FIGURE 8: Novel Tau filaments resemble the heparin-induced Tau filaments that are models for Alzheimer's disease and appear to polymerize from MT ends. All samples used 2 μM Tau and 4 μM MTs incubated for 15 min at 37°C. For the samples in (D) and (E), the MTs were incubated with Tau for 5 min in order to catch the initial stages of the fibrillization process. (A) TEM image of MTs alone. The protofilament ridges can be seen. (B) Heparin-induced Tau filaments: full-length Tau forms a combination of many straight and a few twisted filaments upon incubation with heparin. The inset is a representative image of a Tau-only control: no filament formation was seen over multiple fields and samples. (C) TEM image of the Tau filaments that formed upon incubation with MTs. Note that the ribbon-like, MT-induced Tau filaments in (C) are most similar to the straight, heparin-induced Tau filaments seen in (B) and to others reported previously (Barghorn and Mandelkow, 2002; Jeganathan *et al.*, 2008). Although the MT-induced Tau filaments do not have the periodical twist of the twisted heparin-induced Tau filaments, the MT-induced Tau filaments appear twisted in a braid-like way. (D) Image showing what appears to be a Tau filament polymerizing from an MT end. (E) Image showing a normal blunt MT end at which Tau polymerization is not occurring. (F) Histogram of filament widths. Width measurements were taken as described in *Materials and Methods*. (a) shows the thicker width of MT-induced Tau filaments; (a') shows the thinner width of MT-induced Tau filaments; (b) shows the thicker width of twisted heparin-induced Tau filaments; (b') shows the thinner width of twisted heparin-induced Tau filaments; (c) shows the width of straight heparin-induced Tau filaments; (d) shows the width of MTs. All images shown are representative images of three experiments and were acquired by TEM. Scale bars: 50 nm.

cosedimentation experiments above. We also prepared a control consisting of Tau alone in a heparin-containing buffer that has been classically used to promote the formation of NFT-like filaments (Jeganathan *et al.*, 2008; Ramachandran and Udgaonkar, 2011; Wegmann *et al.*, 2011). As shown in Figure 8A, the MTs in our experiments can be recognized as straight filaments that have clear protofilament ridges. When full-length Tau is incubated with heparin in the NFT-promoting buffer, it forms many straight and a few twisted filaments, in agreement with previous reports (Figure 8B; Wille *et al.*, 1992; Jeganathan *et al.* 2008; Wegmann *et al.*, 2010, 2011; Ramachandran and Udgaonkar, 2011). When Tau is incubated by itself in MT buffer (PEM), no filaments are visible (Figure 8B, inset). However, when Tau and MTs are incubated together, numerous nonhelical filaments without ridges appear (Figure 8C). These filaments appear superficially similar to the classical heparin-induced filaments (compare Figure 8, C and B). Strikingly, we were also able to observe a number of incidences in which the Tau filament appeared to be polymerizing from the MT ends (Figure 8D), in agreement with our previous fluorescence observations (Figure S4).

To conduct a more detailed comparison of the MT-induced and heparin-induced filaments, we measured the widths of the various filaments that occurred in our preparations. The MT-induced Tau filaments were most similar in appearance and width to the straight heparin-induced Tau filaments (Figure 8, B, C, and F). The significance of the slight differences in width between these two types of filaments is not clear, but could be due to buffer conditions. Indeed, many EM studies observing in vitro–generated Tau filaments have shown that the filament morphologies can vary depending on the Tau construct used, the anionic inducer used, or the buffer conditions (Crowther, 1991; Goedert *et al.*, 1992; Barghorn and Mandelkow, 2002; Jeganathan *et al.*, 2008). Recent studies have readdressed the issue of varying Tau filament morphologies and found that the thicker regions of Tau fibrils range between ~9 and 18 nm, and the thinner regions range between ~10 and 15 nm (Wegmann *et al.*, 2010). The observation that the width of the MT-induced Tau filaments falls within these values supports the idea that the MT-induced and heparin-induced filaments are similar structures. Given that the heparin-induced filaments are recognized as models for Alzheimer's-induced NFT filaments, the sum of these data suggest that these MT-induced Tau filaments provide a new in vitro model for Tau NFT formation.

Conclusions

We have found that under the conditions of typical MT-binding assays, MTs induce the rapid formation of novel Tau filaments. The

assembly of these filaments is significant for two reasons. First, we propose that it accounts both for the failure of Tau–MT interactions to fit standard binding models and for the wide ranges of reported affinity values measured under different conditions (Goode and Feinstein, 1994; Sillen *et al.*, 2007; Fauquant *et al.*, 2011). The possibility remains that Tau also binds to MTs in a cooperative manner, as is suggested by the inconsistent nature of the decoration of MTs by Tau (Figure 2). However, it will be difficult to address this issue in a quantitative way until conditions are found that eliminate MT-induced Tau filament formation over a range of Tau concentrations. Questions such as the significance of the Tau purification method for filament formation (i.e., the classic boiling method vs. other approaches) and the mechanism of filament nucleation remain important additional avenues for future research.

The second reason that the formation of MT-induced Tau filaments is significant is that it may have relevance to the function of Tau in both health and disease. First, the observation that Tau forms the filaments rapidly in relatively gentle conditions indicates that Tau–Tau interactions do not require phosphorylation or the presence of chemical inducers. Additionally, the Tau filaments are found to form from the unlabeled protein, as shown by TEM (Figure 8). These observations suggest that Tau–Tau interactions might have a role in normal Tau function. Moreover, the similarity of the MT-induced Tau filaments to those formed in Alzheimer's disease implies that MT induction of Tau filament assembly might provide an easier way to make Tau filaments and thus open new avenues for studying and perhaps inhibiting filament formation. Finally, the induction of Tau filament assembly by MTs in vitro provides additional support for the suggestion (Friedhoff *et al.*, 1998; Ackmann *et al.*, 2000) that MTs might play a role in the formation of Alzheimer's-associated NFTs in vivo.

MATERIALS AND METHODS

Tubulin purification

Tubulin was purified from porcine brain using two polymerization cycles and separation on a P-11 column according to the Mitchison protocol (Mitchison and Kirschner, 1984). Aliquots of purified tubulin were flash-frozen and stored at –80°C.

MT polymerization

Tubulin was assembled into MTs with the stabilizing drug Taxol according to an established protocol (Mitchison and Kirschner, 1984).

Subtilisin digestion of MTs

MT were digested with subtilisin to remove both the α- and β-tubulin tails according to a previously established protocol (Zhu *et al.*, 2009). Removal of both tubulin tails was confirmed by Western blot analysis probed with mouse monoclonal 1A2 anti–α-tubulin antibody (a gift from the lab of Thomas Kreis, University of Geneva), which targets the α-tubulin tail, the second tail to be digested (see Figure S3).

Full-length human Tau

Full-length human Tau protein was recombinantly expressed in *Escherichia coli* BL21(DE3) cells from the vector pRK-172 kindly provided by Khalid Iqbal (Alonso *et al.*, 2010) and purified by the boiling method outlined by Smith *et al.* (2000). Tau concentration was determined by amino acid analysis, and aliquots were stored at –80°C.

Heparin-induced Tau filament formation

Full-length Tau (50 µM) was incubated with 12.5 µM heparin (heparin sodium salt from porcine intestinal mucosa [SKU: H3393; Sigma-Aldrich, St. Louis, MO]) in HEPES buffer (pH 7.6, 10 mM HEPES, 100 mM NaCl, 0.125 mM EDTA, 5 mM dithiothreitol) at 37°C for ~4.5 d (Barghorn and Mandelkow, 2002; Jeganathan *et al.*, 2008).

MT-binding assay

MTs (concentration measured as polymerized tubulin dimers) were incubated at 37°C with Tau protein for 15 min in PEM buffer (100 mM PIPES, pH 6.8, 2 mM $MgCl_2$, 1 mM ethylene glycol tetraacetic acid [EGTA]) supplemented with 10 µM Taxol. The MTs and associated Tau (and any other sedimentable assemblages) were pelleted out of solution at 23,000 × *g* for 20 min at 37°C. The supernatants containing free Tau were separated from the pellets, and the pellets were resuspended in PEM. Samples were mixed with SDS buffer, boiled, and run on a 10% SDS–PAGE gel. Controls with Tau and MTs alone were included in each MT-binding assay. Background-corrected intensities of the bound and free fractions of the Coomassie Blue–stained Tau protein bands were measured using Image J software. GraphPad Prism (La Jolla, CA) was used for all curve fitting, as described below.

Approach TcMv

An MT-binding assay in which the Tau concentration is held constant and the MT concentration is varied over multiple samples run in parallel. Calculations for the data shown assume a 1 Tau:1 tubulin dimer binding ratio (N). The total MT concentrations used were 0, 1, 2, 4, 6, and 8 µM. Data were fitted using nonlinear regression according to Eq. 1, that is, fraction $Tau_{bound} = B_{max}[MT_{free}]/([MT_{free}] + K_D)$, with $B_{max} = 1.0$.

Approach TvMc

An MT-binding assay in which the Tau concentration is varied and the MT concentration is held constant over multiple samples run in parallel. The total Tau concentrations used ranged between 0 and 26 µM. Data were fitted using nonlinear regression according to Eq. 2 or 3, as indicated in the text.

Fluorescence studies

MTs were polymerized using an ~1:3 ratio of carboxytetramethylrhodamine- (TAMRA-) or Alexa Fluor 561–labeled tubulin to unlabeled tubulin; the ratio of dye molecules to tubulin dimers in the labeled tubulin stock solution ranged between 1:5 and 1:3. Tau was labeled with Alexa Fluor 488 (A30052; Invitrogen, Carlsbad, CA), following Invitrogen's protocol for amine-reactive probes. The labeling ratio was generally one dye molecule to ~10 Tau molecules. Labeled Tau generated from multiple different Tau preps formed similar Tau filaments, and control cosedimentation experiments showed that for all preps the binding activity of 2 µM labeled Tau with 2 µM labeled MTs was similar to that of the unlabeled proteins (unpublished data). The labeled MTs and labeled Tau protein were incubated together in BRB80 buffer (80 mM PIPES, pH 6.8, 1 mM $MgCl_2$, 1 mM EGTA) in the presence of 10 µM Taxol; samples were diluted 1:10 and supplemented with an oxygen-scavenging system (mixture containing catalase, glucose oxidase, β-mercaptoethanol, and glucose) just prior to imaging. Images were acquired on a Nikon inverted microscope TE2000 using a 60×/1.4 numerical aperture (NA) objective and a Cascade 512B camera (Photometrics, Tucson, AZ). Figure 4 alone was imaged on a Zeiss Axiovert S100TV inverted microscope using 63×/1.4 NA objective and a Princeton Instruments (Trenton, NJ) Micromax camera. Both microscopes were fitted with a High Q filter set from Chroma (Bellows Falls, VT). All images were

acquired and processed using MetaMorph software (Molecular Devices, Sunnyvale, CA) and further processed using Adobe Photoshop 7.0 (San Jose, CA).

TEM

Images were acquired on a FEI Titan 80-300 D3203 TEM (Hillsboro, OR) at 80 kV and collected by a Gatan camera (Oxford, UK). Samples were fixed with EM-grade glutaraldehyde and spread onto carbon type B, 400-mesh formvar/carbon-coated grids. The grids were previously exposed to Ar/O_2 for 12 s in a Fishione Instruments model 1020 plasma cleaner to make the surfaces hydrophilic. Samples were negatively stained with 2% uranyl acetate.

Filament width measurements

The width of an individual MT-induced Tau filament varies with thicker (Figure 8Fa) and thinner (Figure 8Fa′) regions. Three measurements of the thicker widths along an individual Tau filaments were averaged together to represent the filament's thick width. Three measurements of the thinner widths along an individual Tau filament were averaged together to represent the filament's thin width. The average over multiple filaments (*n*) was taken and is plotted as a bar graph, with the thicker average shown in (Figure 8Fa) and the thinner average shown in (Figure 8Fa′). The same approach was taken to measure the thicker (Figure 8Fb) and thinner (Figure 8Fb′) regions of the heparin-induced, twisted Tau filaments. For the heparin-induced, straight Tau filaments (Figure 8Fc) and for the MTs (Figure 8Fd), three measurements of the width of an individual filament were averaged to count as the individual filament's width. The average over multiple filaments (*n*) was taken and is plotted; the straight heparin-induced Tau filament widths are shown in Figure 8Fc, and the MT widths are shown in Figure 8Fd.

APPENDIX

Discussion and analysis of the binding data in Figure 1

When the value of the dissociation constant for a protein–protein interaction is measured, one protein is typically held constant, while the other is varied, and the data are fitted to an appropriate equation to extract the dissociation constant (more about this later in the Appendix). If the binding is simple, the same answer should be obtained by holding either protein constant in the experiment—it should not matter which is held constant and which is varied. Similarly, the measured affinity should not depend on the concentration of proteins used. We refer to the approach in which Tau concentration, [Tau], is held constant and the concentration of MTs, [MT], is varied as TcMv, and the converse as TvMc. Note that throughout this article, [MT] is measured as the concentration of polymerized tubulin dimers. To test whether differences between the apparent behavior of Tau in the TcMv and TvMc approaches could account for the discrepancies in published Tau–MT affinity values, we measured Tau–MT interactions using both approaches under otherwise identical conditions. To further characterize the interaction, we then tested the dependence of the obtained values on [MT] (in TvMc) and [Tau] (in TcMv). As discussed more below, our results are not only inconsistent with the idea that Tau binds to MTs via a simple interaction, they are also inconsistent with the more sophisticated binding model developed by Ackmann *et al.* (2000), which attempts to incorporate Tau binding to MT-bound Tau. This inconsistency suggests that another interaction not accounted for by the Ackmann model occurs when Tau and MTs are mixed. The main text provides evidence that this "other interaction" is the MT-induced formation of Tau filaments.

Binding of Tau to MTs using the TcMv approach yields a high apparent Tau–MT affinity

Using the TcMv approach, we measured the fraction of a constant amount of Tau that cosediments with different concentrations of Taxol-stabilized MTs. To calculate a K_D value using this approach, one must assume a particular binding ratio between Tau and tubulin and build it into the analysis. This allows one to calculate the concentration of free binding sites on the MTs ($[MT_{free}]$) and to fit the resulting data according to the standard binding Eq. 1 to calculate the Tau–MT K_D apparent (K_{Dapp}), as shown:

$$\text{Fraction Tau bound} = [MT]_{free} / ([MT]_{free} + K_{Dapp}) \quad (1)$$

When we assume a binding ratio (*N*) of 1 Tau:1 tubulin dimer, our data for 1 μM Tau result in an apparent Tau–MT dissociation constant of 0.11 ± 0.02 μM (Figure 1B), in agreement with many reports that Tau binds MTs very tightly (Goode and Feinstein, 1994; Ackmann *et al.*, 2000).

TvMc approach yields a different apparent Tau–MT binding affinity

In parallel to the TcMv experiments described above, we quantified Tau–MT interactions using the TvMc approach. More specifically, we performed experiments in which [MT] was held constant over multiple assays as the amount of Tau was varied, and we measured the amount of Tau that cosedimented with MTs at each [Tau]. By subtracting Tau_{bound} from Tau_{total} in each assay (or, alternatively, by directly measuring the amount of Tau in the supernatant), we ascertained the amount of Tau that remained free ($[Tau]_{free}$). We then used these values and the standard binding equation for the TvMc approach as shown in Eq. 2 to determine the Tau–MT K_D:

$$[Tau]_{bound} = (N[MT][Tau]_{free}) / ([Tau]_{free} + K_{Dapp}) \quad (2)$$

where *N* is the ratio of bound Tau to tubulin dimer (set to be 1 Tau:1 tubulin dimer for all data sets, consistent with the *N* used in the TvMc approach).

We first measured the Tau–MT K_D at 1 μM MTs (Figure 1C) and then compared the data with the theoretical curve (dotted line) that results when Eq. 2 is plotted with the K_{Dapp} value measured by the TcMv approach (Figure 1B). Two major differences between the dotted curve and the data are evident:

1. At low [Tau], the theoretical curve rises much faster than do the actual data points. This observation implies that Tau is binding to MTs more weakly in the TvMc experiments than in the TcMv experiments. Thus, the two approaches do yield different apparent affinities, even when all other variables are held constant.
2. The theoretical curve saturates at 1 μM bound Tau, while the experimental data keep rising in an approximately linear manner well beyond the expected saturation point (as shown by the red arrow in Figure 1C). This second issue makes it impossible to obtain a reasonable fit of Eq. 2 to the data in Figure 1C, regardless of the K_D and *N* values allowed (Figure 1C and unpublished data).

In previous work, Ackmann and colleagues also observed Tau supersaturation, and they attributed this behavior to Tau–Tau interactions occurring at the MT surface (Ackmann *et al.*, 2000). To adjust for this additional interaction, they modified Eq. 2 by adding a linear term to fit the supersaturation of Tau, as shown in Eq. 3:

$$[Tau]_{bound} = (N[MT][Tau]_{free}) / ([Tau]_{free} + K_D) + (1/\rho)[MT][Tau]_{free} \quad (3)$$

where N is the ratio of bound Tau to tubulin dimer (set to be 1 Tau:1 tubulin dimer for all data sets, consistent with the N used in the TcMv approach), and ρ is an additional overloading parameter described by Ackmann *et al.* (2000) as being "formally reminiscent of a K_D value describing a weak affinity of Tau [for Tau]." The first half of Eq. 3 is identical to Eq. 2 and calculates the affinity between the protein and the ligand. The second half of Eq. 3 is a linear term introduced by Ackmann and colleagues to account for the amount of Tau that sediments beyond saturation.

When we fit our data using this biphasic Eq. 3, we obtain a K_D of 2.02 ± 1.03 μM and a ρ of 6.88 ± 0.37 μM (Figure 1C). This K_D value is inconsistent with the K_D = 75 nM reported by Ackmann and colleagues, and it is more than an order of magnitude weaker than the value produced by analysis of the TcMv data (Figure 1B).

The apparent affinity of Tau–MT interactions depends on the concentrations of both Tau and MTs

As seen above, different experimental designs lead to different apparent values for the Tau–MT affinity (Figure 1, B and C). However, differences in method and/or model alone cannot account for the discrepancies in the literature: when comparing the results of the TvMc approach as reported by different research groups, the affinity values still vary more than an order of magnitude from 75 nM to >1 μM (Ackmann *et al.*, 2000; Sun and Gamblin, 2009; Fauquant *et al.*, 2011). One potential explanation for the variation is that the strength of Tau–MT interactions depends on [Tau]. Indeed, such a concentration dependence would be expected from Ackmann's evidence that Tau–Tau interactions can occur at the MT surface. The existence of a Tau concentration dependence could also explain why the apparent affinity depends on the method, because [Tau] is held constant in the TcMv approach, but varies in the TvMc approach.

To test this possibility, we repeated the experiments of Figure 1, B and C, using the same two approaches, but with different concentrations of proteins under otherwise identical conditions. When we changed [Tau] used in the TcMv approach, we found that the apparent Tau–MT affinity also changed (Figure 1D): while 1 μM Tau yielded an apparent affinity of 0.11 ± 0.02 μM (Figure 1B), 2 μM and 4 μM Tau yielded K_{Dapp} values of 1.39 ± 0.35 μM and 0.67 ± 0.16 μM, respectively (Figure 1D). The change in apparent affinity is expected from the idea that Tau binds to Tau on the MT surface (Ackmann *et al.*, 2000), but we were puzzled by the inconsistent nature of the change: the K_D value extracted from the fit rose (i.e., the apparent affinity weakened) from 1 μM to 2 μM Tau and then fell from 2 to 4 μM Tau. It is also notable that the data for the 2 and 4 μM Tau experiments are more variable than the data for the 1 μM Tau. While this variability made it difficult to fit the curves, the general trends observed in Figure 1D were consistent across many experiments (Figure 1D and unpublished data). Possible origins of this variability are discussed more in the main text.

We then studied how Tau–MT interaction measured by the TvMc approach depends on the [MT]. Using Eq. 3 to fit the data and setting N = 1 for consistency, we found that when [MT] changes from 1 to 0.5 to 0.1 μM, the measured K_D changes from 2.02 ± 1.03 μM to 0.84 ± 0.41 μM to 0.10 ± 0.32 μM, respectively (Figure 1E). Moreover, the ρ parameter (described as being similar to an apparent K_D for the Tau–Tau interaction; Ackmann *et al.*, 2000) also changes, ranging from 6.8 ± 0.37 μM at 1 μM MTs to 1.06 ± 0.04 μM at 0.1 μM MTs. Allowing N to vary did not improve the consistency of the extracted K_D or ρ values (unpublished data).

Interpretation of the binding experiments

To yield valid dissociation constants when using standard binding models to fit cosedimentation data, several assumptions must be met. These include the ideas that: 1) Tau–MT binding events are independent and reversible, 2) Tau–MT binding is the only significant interaction occurring in the solution, 3) the interactions have reached equilibrium, and 4) cosedimentation of Tau with MTs reflects the binding of Tau to MTs. Our observation that the apparent affinity depends on the concentration of both Tau and MTs demonstrates that at least one of these assumptions is being violated, and, therefore, that neither Eq. 1 nor Eq. 2 can be validly applied to the Tau–MT cosedimentation data. This conclusion is consistent with that of Ackmann *et al.* (2000), who determined on the basis of TvMc analysis that Tau–Tau interactions are occurring on the MT and Eq. 2 is not sufficient to describe binding of Tau to MTs. To address these issues, Ackmann and colleagues modified Eq. 2 to include a term that attempts to account for the Tau–Tau interactions on the MT surface (Eq. 3). However, we find that even Ackmann's modified binding equation (Eq. 3) is insufficient to describe Tau–MT binding behavior, because the observed K_D and ρ values (implied by Ackmann to be constants) vary with [MT] (Figure 1E). One explanation for these observations is that an as yet unaccounted for interaction is occurring in the Tau–MT binding assays. As discussed in the section of the article on investigations of Tau–Tau interactions, we provide evidence that this additional interaction is the MT-induced formation of Tau-only filaments.

ACKNOWLEDGMENTS

This work was supported by grant MCB-0951264 from the National Science Foundation. We thank William Archer for his technical TEM assistance and the Goodson lab members for insightful discussions.

REFERENCES

Ackmann M, Wiech H, Mandelkow E (2000). Nonsaturable binding indicates clustering of tau on the microtubule surface in a paired helical filament-like conformation. J Biol Chem 275, 30335–30343.

Al-Bassam J, Ozer RS, Safer D, Halpain S, Milligan RA (2002). MAP2 and tau bind longitudinally along the outer ridges of microtubule protofilaments. J Cell Biol 157, 1187–1196.

Alonso AD, Di Clerico J, Li B, Corbo CP, Alaniz ME, Grundke-Iqbal I, Iqbal K (2010). Phosphorylation of Tau at Thr^{212}, Thr^{231}, and Ser^{262} combined causes neurodegeneration. J Biol Chem 285, 30851–30860.

Amos LA (2000). Focusing-in on microtubules. Curr Opin Struct Biol 10, 236–241.

Askham JM, Morrison EE (2002). Evidence that an interaction between EB1 and $p150^{Glued}$ is required for the formation and maintenance of a radial microtubule array anchored at the centrosome. Mol Biol Cell 13, 186A.

Barghorn S, Mandelkow E (2002). Toward a unified scheme for the aggregation of TAU into Alzheimer paired helical filaments. Biochemistry 41, 14885–14896.

Bunker JM, Wilson L, Jordan MA, Feinstein SC (2004). Modulation of microtubule dynamics by tau in living cells: implications for development and neurodegeneration. Mol Biol Cell 15, 2720–2728.

Choi MC *et al.* (2009). Human microtubule-associated-protein tau regulates the number of protofilaments in microtubules: a synchrotron x-ray scattering study. Biophys J 97, 519–527.

Crowther RA (1991). Straight and paired helical filaments in Alzheimer disease have a common structural unit. Proc Natl Acad Sci USA 88, 2288–2292.

Desai A, Mitchison TJ (1997). Microtubule polymerization dynamics. Annu Rev Cell Dev Biol 13, 83–117.

Fauquant C, Redeker V, Landrieu I, Wieruszeski JM, Verdegem D, Laprevote O, Lippens G, Gigant B, Knossow M (2011). Systematic identification of tubulin-interacting fragments of the microtubule-associated protein Tau leads to a highly efficient promoter of microtubule assembly. J Biol Chem 286, 33358–33368.

Friedhoff P, Schneider A, Mandelkow EM, Mandelkow E (1998). Rapid assembly of Alzheimer-like paired helical filaments from microtubule-associated protein tau monitored by fluorescence in solution. Biochemistry 37, 10223–10230.
Goedert M, Jakes R, Crowther RA (1999). Effects of frontotemporal dementia FTDP-17 mutations on heparin-induced assembly of tau filaments. FEBS Lett 450, 306–311.
Goedert M, Spillantini MG, Cairns NJ, Crowther RA (1992). Tau proteins of Alzheimer paired helical filaments—abnormal phosphorylation of all six brain isoforms. Neuron 8, 159–168.
Goode BL, Feinstein SC (1994). Identification of a novel microtubule-binding and assembly domain in the developmentally-regulated inter-repeat region of tau. J Cell Biol 124, 769–782.
Hiraoka S, Yao TM, Minoura K, Tomoo K, Sumida M, Taniguchi T, Ishida T (2004). Conformational transition state is responsible for assembly of microtubule-binding domain of tau protein. Biochem Biophys Res Commun 315, 659–663.
Hirokawa N, Shiomura Y, Okabe S (1988). Tau proteins: the molecular structure and mode of binding on microtubules. J Cell Biol 107, 1449–1459.
Howard J, Hyman AA (2003). Dynamics and mechanics of the microtubule plus end. Nature 422, 753–758.
Jeganathan S, von Bergen M, Mandelkow EM, Mandelkow E (2008). The natively unfolded character of Tau and its aggregation to Alzheimer-like paired helical filaments. Biochemistry 47, 10526–10539.
Kar S, Fan J, Smith MJ, Goedert M, Amos LA (2003). Repeat motifs of tau bind to the insides of microtubules in the absence of taxol. EMBO J 22, 70–77.
Kempf M, Clement A, Faissner A, Lee G, Brandt R (1996). Tau binds to the distal axon early in development of polarity in a microtubule- and microfilament-dependent manner. J Neurosci 16, 5583–5592.
Makrides V, Massie MR, Feinstein SC, Lew J (2004). Evidence for two distinct binding sites for tau on microtubules. Proc Natl Acad Sci USA 101, 6746–6751.
Makrides V, Shen TE, Bhatia R, Smith BL, Thimm J, Lal R, Feinstein SC (2003). Microtubule-dependent oligomerization of tau—implications for physiological tau function and tauopathies. J Biol Chem 278, 33298–33304.
Mitchison T, Kirschner M (1984). Dynamic instability of microtubule growth. Nature 312, 237–242.
Mizushima F, Minoura K, Tomoo K, Sumida A, Taniguchi T, Ishida T (2007). Marked difference between self-aggregations of first and fourth repeat peptides on tau microtubule-binding domain in acidic solution. J Biochem 142, 49–54.
Panda D, Goode BL, Feinstein SC, Wilson L (1995). Kinetic stabilization of microtubule dynamics at steady-state by tau and microtubule-binding domains of tau. Biochemistry 34, 11117–11127.
Paudel HK, Li W (1999). Heparin-induced conformational change in microtubule-associated protein tau as detected by chemical cross-linking and phosphopeptide mapping. J Biol Chem 274, 8029–8038.
Philip JT, Pence CH, Goodson HV (2012). MTBindingSim: simulate protein binding to microtubules. Bioinformatics 28, 441–443.
Ramachandran G, Udgaonkar JB (2011). Understanding the kinetic roles of the inducer heparin and of rod-like protofibrils during amyloid fibril formation by Tau protein. J Biol Chem 286, 38948–38959.
Schaap IAT, Hoffmann B, Carrasco C, Merkel R, Schmidt CF (2007). Tau protein binding forms a 1 nm thick layer along protofilaments without affecting the radial elasticity of microtubules. J Struct Biol 158, 282–292.
Sillen A, Barbier P, Landrieu I, Lefebvre S, Wieruszeski JM, Leroy A, Peyrot V, Lippens G (2007). NMR investigation of the interaction between the neuronal protein Tau and the microtubules. Biochemistry 46, 3055–3064.
Slaughter T, Wang J, Black MM (1997). Microtubule transport from the cell body into the axons of growing neurons. J Neurosci 17, 5807–5819.
Smith MJ, Crowther RA, Goedert M (2000). The natural osmolyte trimethylamine N-oxide (TMAO) restores the ability of mutant tau to promote microtubule assembly. FEBS Lett 484, 265–270.
Sun Q, Gamblin TC (2009). Pseudohyperphosphorylation causing AD-like changes in Tau has significant effects on its polymerization. Biochemistry 48, 6002–6011.
Tanaka EM, Kirschner MW (1991). Microtubule behavior in the growth cones of living neurons during axon elongation. J Cell Biol 115, 345–363.
Wegmann S, Jung YJ, Chinnathambi S, Mandelkow E-M, Mandelkow E, Muller DJ (2010). Human tau isoforms assemble into ribbon-like fibrils that display polymorphic structure and stability. J Biol Chem 285, 27302–27313.
Wegmann S, Scholer J, Bippes CA, Mandelkow E, Muller DJ (2011). Competing interactions stabilize pro- and anti-aggregant conformations of human tau. J Biol Chem 286, 20512–20524.
Wille H, Drewes G, Biernat J, Mandelkow E-M, Mandelkow E (1992). Alzheimer-like paired helical filaments and antiparallel dimers formed from microtubule-associated protein tau in vitro. J Cell Biol 118, 573–584.
Witte H, Neukirchen D, Bradke F (2008). Microtubule stabilization specifies initial neuronal polarization. J Cell Biol 180, 619–632.
Zhu ZQC, Gupta KK, Slabbekoorn AR, Paulson BA, Folker ES, Goodson HV (2009). Interactions between EB1 and microtubules: dramatic effect of affinity tags and evidence for cooperative behavior. J Biol Chem 284, 32651–32661.